Journal of Thermal Analysis and Calorimetry (2020) 140:645–655
https://doi.org/10.1007/s10973-019-08903-4

Characterization of ignition and combustion characteristics of phenolic fiber-reinforced plastic with different thicknesses

Ruiyu Chen[1,2,3] · Xiaokang Xu[1] · Yang Zhang[4] · Shouxiang Lu[2] · Siuming Lo[3]

Received: 20 May 2018 / Accepted: 5 October 2019 / Published online: 30 October 2019

Abstract

The present study focuses on ignition and combustion characteristics of phenolic fiber-reinforced plastic (FRP) with different thicknesses under different external heat fluxes using cone calorimeter, which receives little attention to date. A series of parameters including ignition time, thermal thickness, mass loss factor, mass loss rate (MLR), heat release rate (HRR), total heat release (THR), fire performance index (FPI) and fire growth index (FGI) are measured or calculated. Results indicate that the ignition time increases with the thickness, but decreases with the external heat flux. Phenolic FRP with thickness of 3 mm may be considered as thermally thin material. However, phenolic FRP with thickness of 5 and 8 mm is prone to be thermally thick material. The critical heat flux, minimum heat flux and ignition temperature are deduced and validated. The thermal thickness increases with the external heat flux. Linear correlations of the thermal thickness with the ratio of specimen density and external heat flux are demonstrated and presented. The mass loss factor decreases with the thickness. Three and two peak MLRs occur in the cases of low and high external heat fluxes, respectively. The average MLR increases with the external heat flux and thickness. The average and maximum HRR increases with the external heat flux. The FGI for the maximum HRR increases with the external heat flux. Linear correlations of the average MLR, the average and maximum HRR and the FGI for the maximum HRR with the external heat flux are demonstrated and presented.

Keywords Thickness · Cone calorimeter · Ignition characteristics · Combustion · Correlation · Phenolic FRP

Introduction

Phenolic fiber-reinforced plastic (FRP) is a typical thermosetting plastic. Owing to its prominent thermal insulation, outstanding impact resistance, and sound absorption characteristics, it is increasingly used as interior materials for buildings, aircrafts, ships, automobiles, etc. However, the fire hazard of phenolic FRP is relatively high, which may restrict its application range. It can be ignited and released large amounts of heat and poisonous gases, especially under high external heat fluxes or high-temperature conditions, such as the case of severe arson, probably involving in the combustion of other neighboring flammable materials, resulting in terrible casualties and property loss. Therefore, it is necessary and important to investigate the ignition and combustion characteristics of phenolic FRP, which are the key elements in the fire hazard evaluation of phenolic FRP.

Generally, solid combustibles can be divided into thermally thick or thermally thin material according to whether the physical thickness of the specimen is larger or less than the thermal thickness at ignition moment. If the solid combustibles are considered as thermally thick materials, heterogeneous temperature profile occurs inside the solid when they are exposed to heat. If the solid combustibles are regarded as thermally thin materials, temperature distributes almost homogeneously inside the solid when they are exposed to heat. Obviously, large differences may

✉ Ruiyu Chen
crynjust@njust.edu.cn

1 School of Chemical Engineering, Nanjing University of Science and Technology, Nanjing 210094, Jiangsu, People's Republic of China

2 State Key Laboratory of Fire Science, University of Science and Technology of China, Hefei 230027, Anhui, People's Republic of China

3 Department of Civil and Architectural Engineering, City University of Hong Kong, Kowloon 999077, Hong Kong, People's Republic of China

4 School of Science, Nanjing University of Science and Technology, Nanjing 210094, Jiangsu, People's Republic of China

occur to the ignition and combustion characteristics of thermally thick and thermally thin materials. As a result, studies regarding the influence of thickness on the ignition and combustion characteristics of solid combustibles, such as PS (polystyrene) [1] and oil-impregnated transformer insulating paperboard [2], have been reported employing cone calorimeter [3–11].

Some studies focused on the ignition and combustion characteristics of phenolic FRP. Mouritz et al. [12, 13] measured the ignition time of phenolic FRP under the external heat flux range of 25–100 kW m^{-2} employing cone calorimeter. However, combustion characteristics of phenolic FRP were not investigated in their study. In addition, Avila [14] investigated the effects of resin and glass content on the ignition and combustion characteristics of phenolic FRP under single external heat flux of 70 kW m^{-2} using cone calorimeter, which is generally used for determination of the ignition and combustion characteristics of solid combustibles [15, 16]. Ignition time, mass loss rate (MLR) and heat release rate (HRR) were measured to reveal the differences of the ignition and combustion characteristics of phenolic FRP with different resin and glass contents. Similarly, Ramsay et al. [17] performed a study on the influence of resin and glass content on the ignition and combustion characteristics of phenolic FRP under the external heat fluxes of 35, 50 and 75 kW m^{-2} employing cone calorimeter. It should be noted that in the research of Avila [14] and Ramsay et al. [17], the effects of external heat flux on the ignition and combustion characteristics of phenolic FRP were not revealed. Besides, Duggan [18] measured the HRR of painted phenolic FRP under the external heat flux of 35 kW m^{-2}. Effects of external heat flux on the ignition and combustion characteristics of phenolic FRP were not revealed either. It should be noted that all the above-mentioned studies did not focus on the effects of thickness on the ignition and combustion characteristics of phenolic FRP.

In summary, the effects of external heat flux and thickness on the ignition and combustion characteristics of phenolic FRP have not been revealed yet to date. The present study employs cone calorimeter to investigate the ignition and combustion characteristics of phenolic FRP with different thicknesses under different external heat fluxes. A series of parameters including ignition time, thermal thickness, mass loss factor, MLR, HRR, total heat release (THR), fire performance index (FPI) and fire growth index (FGI) are measured. The above-mentioned ignition and combustion parameters under different thicknesses and external heat fluxes are compared and analyzed. Correlations of the above ignition and combustion characteristics with the external heat fluxes are established. The critical heat flux, minimum heat flux and ignition temperature are deduced and validated.

Experimental

Materials

The phenolic FRP used for the present study was provided by Shanghai FRP Research Institute. According to the technical data of the specimen provided by the supplier, the phenolic FRP consists of approximately 50% phenolic resin and 50% fiberglass (mass fraction). Phenolic resin in the phenolic FRP was obtained by condensation polymerization of phenol and formaldehyde. The fundamental properties of the phenolic FRP including the specific heat, the thermal conductivity, the thermal diffusivity, the density and the ignition temperature are shown in Table 1. The values of the density ρ and the ignition temperature were provided by the supplier. The specific heat c, the thermal conductivity λ and the thermal diffusivity α were measured using a hot-disk TPS2500 s. The thickness of the specimen used in the present study is 3, 5 and 8 mm, which are the common thickness of phenolic FRP composite in end use.

Measurement

The cone calorimeter experiments were carried out using an ISO 5660-1 standard Cone Calorimeter with a digital electronic balance (UX6200H) with the accuracy of 0.01 g. The specimen with the dimension of 100 × 100 mm was used for the experiments. In order to eliminate the mass transfer along all the boundaries except the exposed face of the specimen to the external heat source, aluminum foil was used to wrap the edges and rear surface of the specimen. In addition, to prevent the specimen from intumescing, a wire grid which was made of 2-mm stainless steel rod with all intersections welded was used. Ceramic fiber blanket was positioned underneath the specimen for thermal insulation. The specimen along with the specimen holder was positioned horizontally on a lifting platform. The distance between the cone heater and the top surface of the specimen was 25 mm. External heat fluxes including 30, 35, 40, 45, 50, 55, 60 and 65 kW m^{-2} were selected. Experiments were conducted with the ambient temperature of 298 ± 2 K and the relative humidity of 50 ± 5%. Cone calorimeter

Table 1 Fundamental properties of phenolic FRP

Elements	Value
Specific heat c/J kg^{-1} K^{-1}	735.93
Thermal conductivity λ/W m^{-1} K^{-1}	0.36
Thermal diffusivity α/m^2 s^{-1}	2.97×10^{-7}
Density ρ/kg m^{-3}	1.63
Ignition temperature/K	803

was calibrated following the standard of ISO 5660-1 [19] before each test. Experiment was terminated manually if no ignition occurred in 32 min following the standard of ISO 17554 [20].

Results and discussion

Ignition characteristics

Ignition time is one of the key parameters to characterize the fire hazard and thermal decomposition behaviors of solid combustibles. In general, specimen with high ignition time has low fire hazard and high thermal resistance. Correlation of the ignition time with the applied external heat flux can be used to determine whether the specimen behaves as thermally thick material or thermally thin material [21–24]. Moreover, correlation of the ignition time with the applied external heat flux may be used to obtain the flammability properties of solid combustibles, such as the critical heat flux (CHF) and the ignition temperature.

The ignition time as a function of external heat flux in the case of different thicknesses is presented in Fig. 1a. The ignition time corresponds to the start moment of the occurrence of sustained flaming instead of transitory flaming according to the flame image record. It should be noted that ignition did not occur in the case of 30 kW m^{-2}. As shown in Fig. 1a, the ignition time decreases with the external heat flux. Besides, the ignition time increases with the thickness under the identical external heat flux. It may be due to that more energy is required for the decomposition of the thicker specimen, and more time is required to achieve the lower flammable limit of the combustible gases generated by the decomposition of the specimen. Furthermore, with the increase in the external heat flux, the difference of the ignition time under different thicknesses in the case of the identical external heat flux decreases with the external heat flux.

Based on Quintiere's model [21], correlation of the ignition time with the applied external heat flux may be used to determine whether the specimen behaves as thermally thick or thermally thin material when it is exposed to heat. The specific procedure is illustrated as follows:

1. Correlation of the transformed ignition time $(1/t_{ig})^n$ with the applied external heat flux using different values of n (t_{ig} denotes the ignition time. n is a coefficient. $n=0.5$ and 1 correspond to the cases of thermally thick and thermally thin materials, respectively).
2. The least-squares method is used to obtain the value of the correlation coefficient R^2. The value of n with higher R^2 is adopted. Based on the value of n, whether

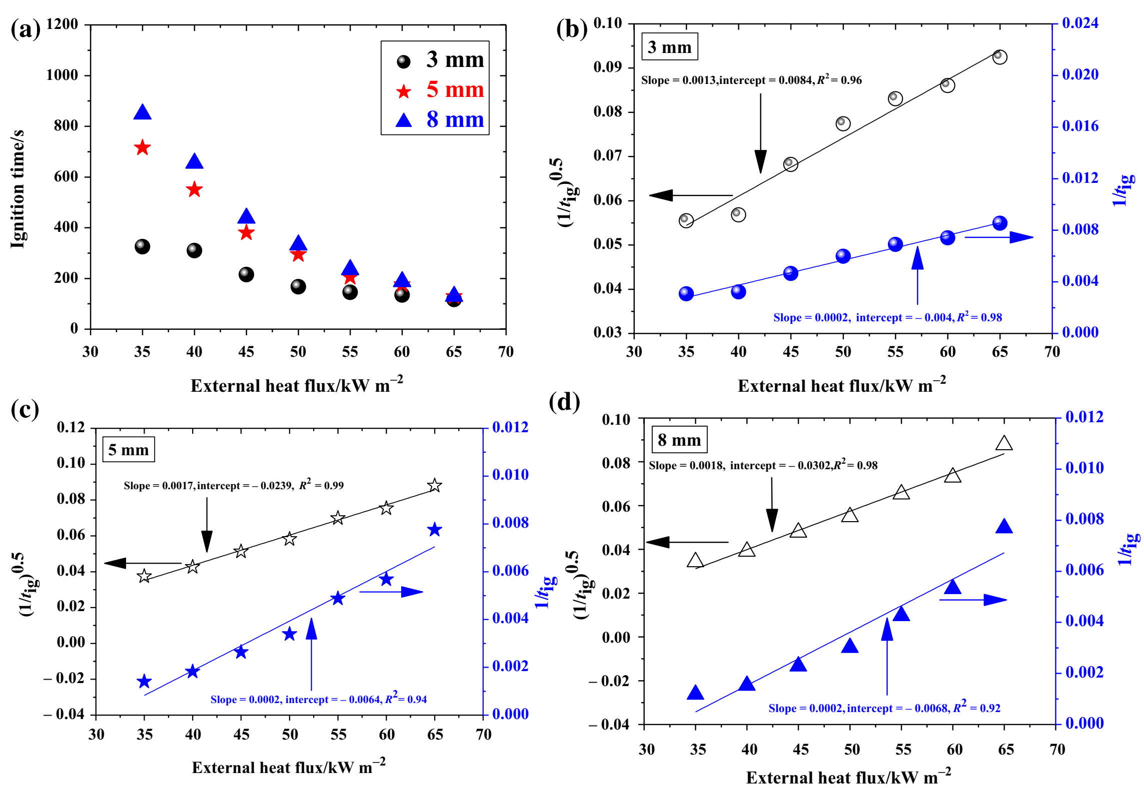

Fig. 1 Ignition time versus external heat flux under different thicknesses

the specimen behaves as thermally thick or thermally thin material may be determined.

Figure 1b–d shows the correlation of the transformed ignition time $(1/t_{ig})^n$ with the applied external heat flux under different thicknesses. The values of the slope and the intercept of the fitting line as well as the correlation coefficient are presented. According to Quintiere's model [21], the specimen with the thickness of 3 mm is prone to be thermally thin material. However, the specimen with the thickness of 5 and 8 mm may be considered as thermally thick material.

Based on the opinions of Quintiere [21] and Luche et al. [22, 23], the value of the theoretical CHF $\dot{q}''_{cr}$ can be calculated using Eq. (1). Thus, the value of the theoretical CHF $\dot{q}''_{cr}$ in the cases of 3, 5 and 8 mm is calculated to be 20, 14.1 and 16.8 kW m^{-2}, respectively. The average value of $\dot{q}''_{cr}$ for the three cases is about 16.9 kW m^{-2}.

$$\mathrm{CHF} = \left[-\frac{hboxIntercept}{\mathrm{Slope}}\right] \tag{1}$$

Besides the theoretical CHF $\dot{q}''_{cr}$, the minimum heat flux $\dot{q}''_{min}$ is also generally used to evaluate the ignition characteristics of solid combustibles. It should be noted that $\dot{q}''_{cr}$ is generally determined from the curve-fitting of the ignition time with the applied external heat flux. However, $\dot{q}''_{min}$ denotes the heat flux which is just sufficient to heat the material surface to attain the ignition temperature for considerably long exposure times (theoretically ∞) [22]. For engineering purpose, $\dot{q}''_{min}$ may be considered as the average value of the lowest external heat flux at which ignition occurs and the highest external heat flux at which no ignition occurs for 32 min [20, 25]. Thus, the value of $\dot{q}''_{min}$ is calculated to be 32.5 kW m^{-2} in the present study. The ratio of $\dot{q}''_{cr}$ and $\dot{q}''_{min}$ in the cases of 3, 5 and 8 mm is 0.62, 0.44 and 0.52, respectively, which is consistent with the results found in the literature (0.11–0.7) [25, 26]. In addition, based upon $\dot{q}''_{min}$, the ignition temperature is calculated to be 813 K from Eq. (2) using a MATLAB program, which is almost consistent with the experimental measured one (803 K), as presented in Table 1 in "Materials" section.

$$\varepsilon \dot{q}''_{\min} = h_c\left(T_{ig} - T_\infty\right) + \varepsilon\sigma\left(T_{ig}^4 - T_\infty^4\right) \tag{2}$$

where h_c denotes the convective heat transfer coefficient and is taken as 0.0135 kW m^{-2} K^{-1} [25] in the present study. ε denotes the surface emissivity of the specimen at ignition moment and is taken as 0.88 [25] in the present study. σ is the Stefan–Boltzmann constant (5.67×10^{-11} kW m^{-2} K^{-4}). T_{ig} and T_∞ denote the ignition temperature of the specimen and the ambient temperature (K), respectively.

Thermal thickness

The thermal thickness represents the thermal penetration depth at ignition moment, which is defined as the thickness of the specimen which has been heated to a certain temperature at ignition moment [25]. The thermal thickness can be calculated based on Eq. (3) [25]:

$$\delta_P = A\sqrt{\frac{\lambda t_{ig}}{\rho c}} \tag{3}$$

where δ_P denotes the thermal thickness of the specimen (m). A is a constant and taken as 1 in the present study based on the work of Mikkola and Wichman [27]. λ, ρ and c are the thermal conductivity (W m^{-1} K^{-1}), the density (kg m^{-3}) and the specific heat (J kg^{-1} K^{-1}) of the specimen, respectively.

In addition to Eq. (3), the thermal thickness of the specimen may be also estimated using Eq. (4) [25].

$$\delta_P = B\frac{\rho}{\dot{q}''_e} + C \tag{4}$$

where both of B and C are constant. $\dot{q}''_e$ denotes the external heat flux (kW m^{-2}).

Obviously, it is easier to obtain the value of the thermal thickness using Eq. (4) than Eq. (3) since Eq. (4) merely needs to know the specimen density and the applied external heat flux, and these two parameters are quite easy to get. Thus, the results based on Eqs. (3) and (4) are correlated and shown in Fig. 2. It can be seen from Fig. 2 that the thermal thickness δ_P is proportional to $\rho/\dot{q}''_e$ and high correlation coefficient R^2 is demonstrated in the cases of 3, 5 and 8 mm. In addition, little differences occur between the values of δ_P in the cases of 5 and 8 mm. Thus, the values of δ_P in the cases of 5 and 8 mm may be correlated with the

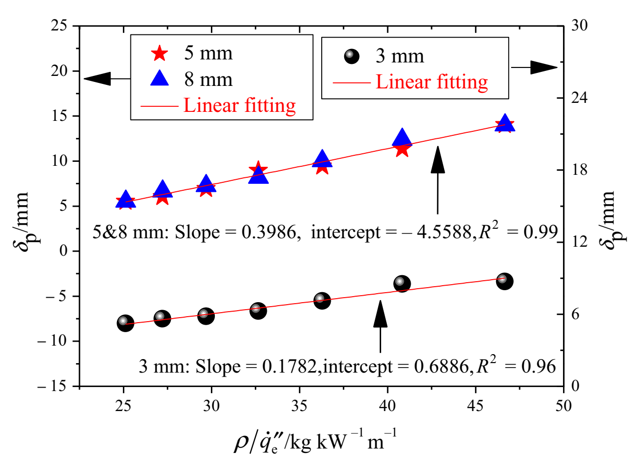

Fig. 2 Correlation among thermal thickness, density and external heat flux under different thicknesses

external heat flux together. The large differences between the cases of 3 mm and 5, 8 mm are resulted by that the specimen with thickness of 3 mm is prone to be thermally thin material in which temperature distributes almost homogeneously when exposed to external heat [28]. However, the specimen with thickness of 5 and 8 mm may be considered as thermally thick material where heterogeneous temperature profile occurs when exposed to external heat [28]. The correlation for the thermally thick specimen (5 and 8 mm) and thermally thin specimen (3 mm) is expressed as Eqs. (5) and (6), respectively.

$$\delta_{\mathrm{Pthick}} = 0.3986\rho / \dot{q}''_{\mathrm{e}} - 4.5588 \tag{5}$$

$$\delta_{\mathrm{Pthin}} = 0.1782\rho / \dot{q}''_{\mathrm{e}} + 0.6886 \tag{6}$$

where δ_{Pthick} and δ_{Pthin} denote the thermal thickness in the cases of thermally thick (5 and 8 mm) and thermally thin phenolic FRP (kW s^{-1} m^{-2}), respectively.

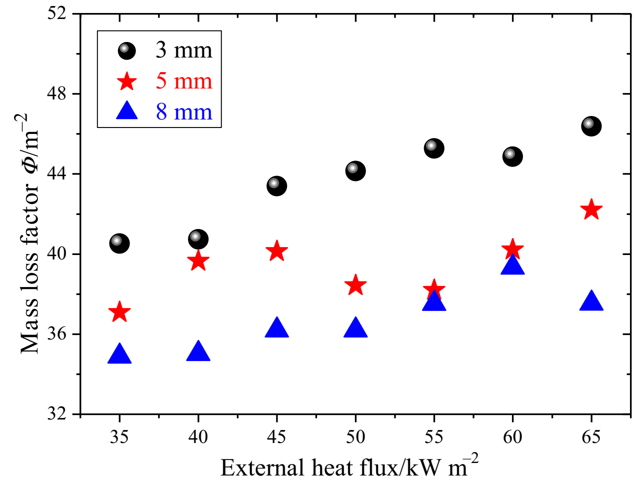

Fig. 3 Mass loss factor versus external heat flux under different thickness

Mass loss factor and mass loss rate

Mass loss factor

Mass loss factor ϕ denotes the ratio of the total mass loss and the initial mass per unit area of the specimen [29]. It can be expressed as Eq. (7).

$$\phi = \frac{m_0 - m}{m_0 A} \tag{7}$$

where m_0, m and A denote the initial mass (kg), the residue mass (kg) and the area of the specimen exposed to the cone heater (m^2), respectively.

Figure 3 shows the mass loss factor ϕ as a function of external heat flux in the cases of 3, 5 and 8 mm. It is indicated that ϕ decreases with the thickness under the identical external heat flux. This may be due to that more complete burning occurs in the specimen with smaller thickness.

Mass loss rate

Mass loss rate (MLR) is defined as the mass rate of solid or liquid fuel vaporized and burned [29]. It can be used to characterize the decomposition rate of the specimen and thus evaluate its fire hazard. Figure 4a–c shows the MLR against time under typical external heat flux and different thicknesses. It is indicated in Fig. 4a that there are three peaks under 35 kW m^{-2} for the cases of 3, 5 and 8 mm. However, as shown in Fig. 4b, in the case of 50 kW m^{-2}, there are two peaks in the cases of 3 and 5 mm, while there are three peaks in the case of 8 mm. With the continuing increase in the external heat flux to 65 kW m^{-2}, as shown in Fig. 4c, there are two peaks for the cases of 3, 5 and 8 mm. This may be due to that: After ignition, char layer was generated in the combustion process and prevented the continuing combustion. In the case of low external heat fluxes, the heat was not sufficient to rapidly penetrate into the char layer, leading to the decrease in MLR and the generation of the second peak MLR. However, in the case of high external heat fluxes, the heat was high enough to rapidly penetrate into the char layer and the continuing combustion may be maintained. The second peak MLR consequently disappeared. It should be noted that more char was generated in the case of 8 mm in comparison with that of 3 and 5 mm. It may need more time to penetrate into the generated char layer. As a consequence, just as Fig. 4b shows, three peaks occur in the case of 8 mm, while merely two peaks occur in the cases of 3 and 5 mm.

Table 2 presents the average MLR under different external heat fluxes and thicknesses. Correlation of the average MLR with the external heat flux under different thicknesses is presented in Fig. 4d. As shown in Table 2 and Fig. 4d, the average MLR increases with the external heat flux and the thickness. The correlation of the average MLR with the external heat flux in the cases of 3, 5 and 8 mm is different, as presented as follows.

$$\bar{\dot{m}}''_{\mathrm{a3}} = 0.0299\dot{q}''_{\mathrm{e}} + 0.5434 \tag{8}$$

$$\bar{\dot{m}}''_{\mathrm{a5}} = 0.0373\dot{q}''_{\mathrm{e}} + 0.3893 \tag{9}$$

$$\bar{\dot{m}}''_{\mathrm{a8}} = 0.0569\dot{q}''_{\mathrm{e}} + 0.1144 \tag{10}$$

where $\bar{\dot{m}}''_{\mathrm{a3}}$, $\bar{\dot{m}}''_{\mathrm{a5}}$ and $\bar{\dot{m}}''_{\mathrm{a8}}$ denote the average MLR of the specimen with the thickness of 3, 5 and 8 mm (g s^{-1} m^{-2}), respectively.

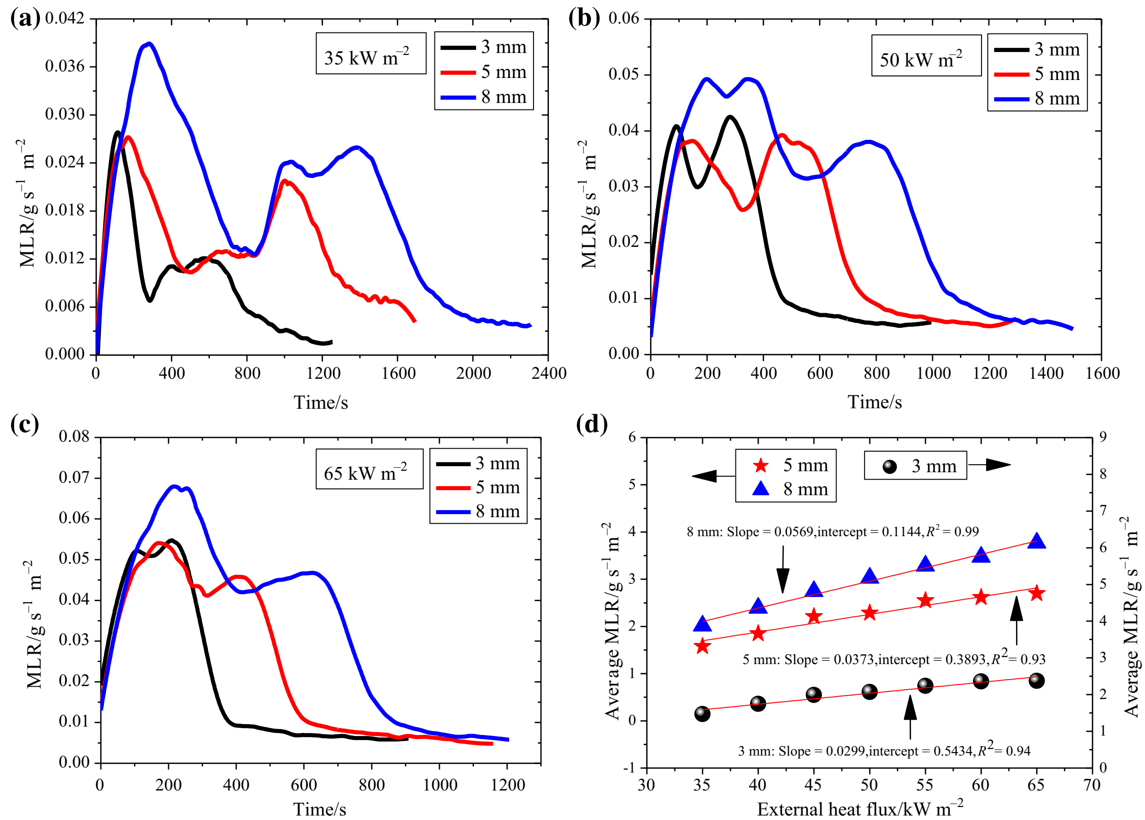

Fig. 4 Typical MLR versus time: **a** 35 kW m^{-2}, **b** 50 kW m^{-2} and **c** 65 kW m^{-2}, and **d** average MLR versus external heat flux under different thicknesses

Table 2 Average MLR data

External heat flux/ kW m^{-2}	Average MLR/g s^{-1} m^{-2}		
	3 mm	5 mm	8 mm
35	1.4705	1.7069	2.0162
40	1.7495	2.0446	2.3933
45	1.9927	2.2129	2.7444
50	2.0703	2.3153	3.0275
55	2.2361	2.5504	3.2835
60	2.3603	2.6451	3.4734
65	2.3757	2.7923	3.7709

Heat release rate and total heat release

Heat release rate

Heat release rate (HRR) denotes the rate of thermal energy released from the combustion of the solid combustibles and is considered as the single most important variable in fire hazard evaluation [22, 23, 30]. The oxygen consumption calorimetry technique based on ISO 5660-1 standard [19, 30–32] was used to calculate the HRR by measuring the concentration of gaseous compounds (O_2, CO_2, CO, etc.) generated by the combustion of the specimen.

Figure 5a–c illustrates the HRR against time under typical external heat flux in the cases of 3, 5 and 8 mm. As shown in Fig. 5a–c, after ignition, a quasi-steady stage occurs before the HRR attains its maximum value. The occurrence of the quasi-steady stage may be due to the formation of the char layer. The gradual increase stage between the quasi-steady stage and the maximum HRR may be resulted by the crack of the formed char layer. In addition, it is indicated in Fig. 5 that the increase in the maximum HRR with the external heat flux in the case of 3 mm is larger than that of 5 and 8 mm. This phenomenon may be resulted by that the specimen with the thickness of 3 mm is prone to be thermally thin material in which temperature distributes almost homogeneously when exposed to external heat [28]. However, the specimen with thickness of 5 and 8 mm may be considered as thermally thick material where heterogeneous temperature profile occurs when exposed to external heat [28]. With the increase in the external heat flux, it is easier for the specimen with the thickness of 3 mm to attain heat balance than that of 5 and 8 mm. The combustion efficiency in the case of 3 mm is larger than that of 5 and 8 mm.

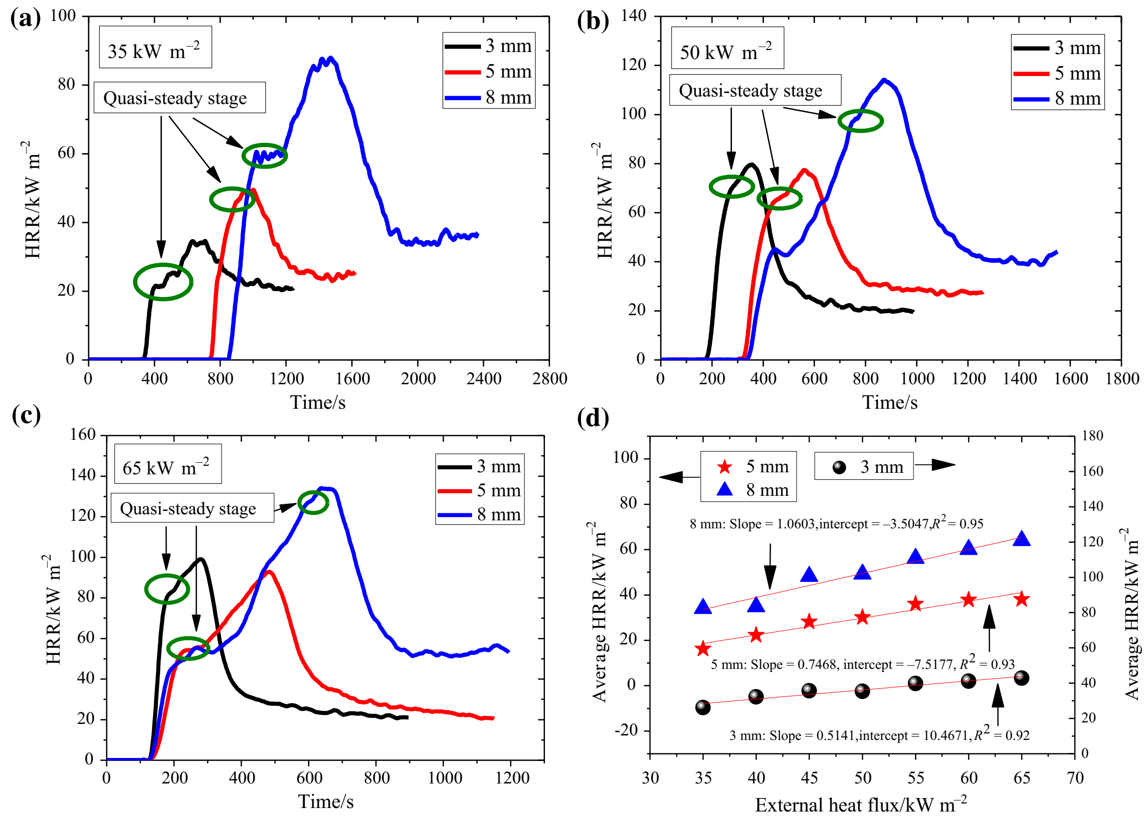

Fig. 5 Typical HRR versus time: **a** 35 kW m^{-2}, **b** 50 kW m^{-2} and **c** 65 kW m^{-2}, and **d** average HRR versus external heat flux under different thicknesses

Table 3 Average HRR under different thicknesses and external heat fluxes

External heat flux/kW m^{-2}	Average HRR/kW m^{-2}		
	3 mm	5 mm	8 mm
35	26.1529	16.2457	34.0264
40	32.2438	22.2521	34.8392
45	35.6598	28.1409	48.1959
50	35.3601	30.1592	49.2479
55	39.7958	36.0601	56.1526
60	41.1417	37.8269	60.0656
65	42.8311	38.0738	64.0362

Table 3 presents the average HRR under different external heat fluxes in the cases of 3, 5 and 8 mm. The correlation of the average HRR with the external heat flux in the cases of 3, 5 and 8 mm is presented in Fig. 5d. As illustrated in Table 3 and Fig. 5d, the average HRR increases with the external heat flux. In addition, the average HRR in the case of 5 mm is the lowest and the average HRR in the case of 8 mm is the highest. This may be due to that the specimen with the thickness of 3 mm behaves as thermally thin material, while the specimens with the thickness of 5 and 8 mm are prone to be thermally thick materials, as noted in "Ignition characteristics" section. Compared with the case of 5 mm, more homogeneous temperature profile occurs inside the specimen with the thickness of 3 mm, generating larger HRR with more complete burning and higher combustion efficiency. However, when the thickness of the specimen is increased from 5 mm to 8 mm, more quantity of specimen is decomposed and more flammable gases for combustion are generated consequently. The quantity of the specimen instead of the combustion efficiency becomes the dominating factor influencing the HRR. The correlation of the average HRR with the external heat flux in the cases of 3, 5 and 8 mm is different, as presented in the following.

$$\bar{\dot{q}}''_{a3} = 0.5141\dot{q}''_{e} + 10.4671 \quad (11)$$

$$\bar{\dot{q}}''_{a5} = 0.7468\dot{q}''_{e} - 7.5177 \quad (12)$$

$$\bar{\dot{q}}''_{a8} = 1.0603\dot{q}''_{e} - 3.5047 \quad (13)$$

where $\bar{\dot{q}}''_{a3}$, $\bar{\dot{q}}''_{a5}$ and $\bar{\dot{q}}''_{a8}$ denote the average HRR in the cases of 3, 5 and 8 mm (kW m^{-2}), respectively.

Table 4 presents the maximum HRR under different external heat fluxes in the cases of 3, 5 and 8 mm. The correlation of the maximum HRR with the external heat

Table 4 Maximum HRR and corresponding time under different thicknesses and external heat fluxes

External heat flux/kW m^{-2}	Maximum HRR/kW m^{-2}/time/s		
	3 mm	5 mm	8 mm
35	34.6201/707	49.518/1005	87.9587/1472
40	47.8517/591	58.1471/1046	90.8257/1034
45	64.4606/522	72.5199/672	107.6306/906
50	79.6076/352	77.3637/556	114.1576/869
55	90.1449/348	83.3135/486	121.5133/766
60	92.2089/299	88.7529/508	128.7522/751
65	99.0911/278	92.8354/483	134.1064/640

flux in the cases of 3, 5 and 8 mm is presented in Fig. 6. As illustrated in Table 4 and Fig. 6, the maximum HRR increases with the external heat flux and the thickness in the cases of external heat flux ≤ 45 kW m^{-2}. However, in the cases of external heat flux > 45 kW m^{-2}, similar to the case of the average HRR as presented in Table 3, the maximum HRR in the case of 5 mm is the lowest and the maximum HRR in the case of 8 mm is the highest. The correlation of the maximum HRR with the external heat flux in the cases of 3, 5 and 8 mm is presented as follows.

$$\dot{q}''_{m3} = 2.1987\dot{q}''_{e} - 37.3635 \tag{14}$$

$$\dot{q}''_{m5} = 1.4426\dot{q}''_{e} + 2.5082 \tag{15}$$

$$\dot{q}''_{m8} = 1.6299\dot{q}''_{e} + 30.6425 \tag{16}$$

where $\dot{q}''_{m3}$, $\dot{q}''_{m5}$ and $\dot{q}''_{m8}$ denote the maximum HRR in the cases of 3, 5 and 8 mm (kW m^{-2}), respectively.

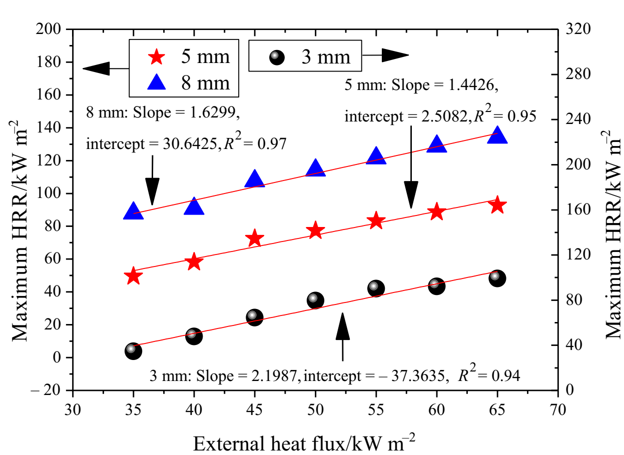

Fig. 6 Maximum HRR versus external heat flux under different thicknesses

Total heat release

Total heat release (THR) denotes the total thermal energy released from the combustion of the solid combustibles and is sometimes used for the fire hazard evaluation. Figure 7 illustrates the THR as a function of external heat flux under different thicknesses. It is indicated that the THR increases with the thickness and the external heat flux.

Fire performance index and fire growth index

Fire performance index

Fire performance index (FPI) is generally used to characterize the fire hazard of solid combustibles. Solid combustibles with high fire hazard possess high FPI value. The value of FPI can be calculated by the following equation:

$$\mathrm{FPI} = \mathrm{pkHRR}/t_{ig} \tag{17}$$

where pkHRR denote the peak HRR (kW m^{-2}).

Figure 8 shows the FPI for the maximum HRR FPI_m versus external heat flux under different thicknesses. More detailed information is presented in Table 5. As illustrated in Fig. 8 and Table 5, the value of FPI_m increases gradually with the external heat flux in the cases of 5 mm and 8 mm. However, little variations of the value of FPI_m with the external heat flux occur in the cases of 3 mm.

Fire growth index

Fire growth index (FGI) is generally used to characterize the fire development rate after ignition from the perspective of heat release. High fire hazard of material is indicated if the value of FGI is high. FGI is expressed as follows:

$$\mathrm{FGI} = \mathrm{pkHRR}/t_{pkHRR} \tag{18}$$

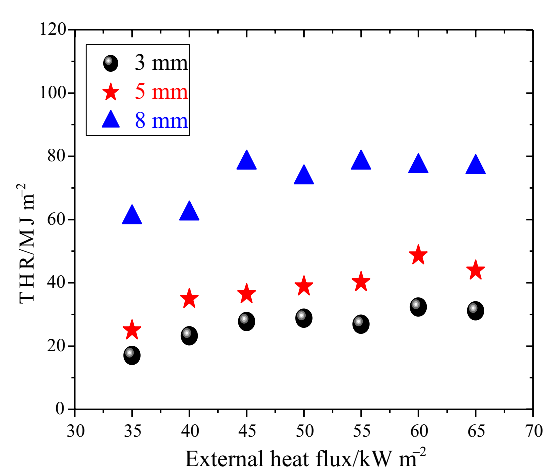

Fig. 7 THR versus external heat flux under different thicknesses

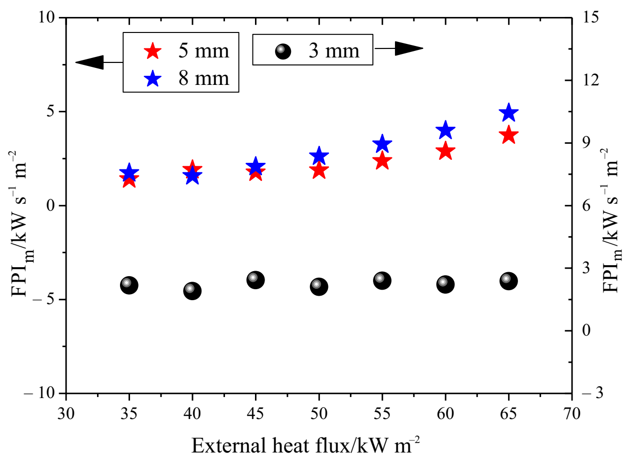

Fig. 8 FPI_m versus external heat flux under different thickness

Table 5 FPI_m data under different thicknesses and external heat fluxes

External heat flux/ kW m^{-2}	FPI_m/kW s^{-1} m^{-2}		
	3 mm	5 mm	8 mm
35	2.1754	1.4056	1.7338
40	1.9065	1.9018	1.5786
45	2.4279	1.7684	2.0685
50	2.1078	1.8847	2.6175
55	2.4000	2.3707	3.2596
60	2.2148	2.8864	3.9947
65	2.37607	3.7442	4.9231

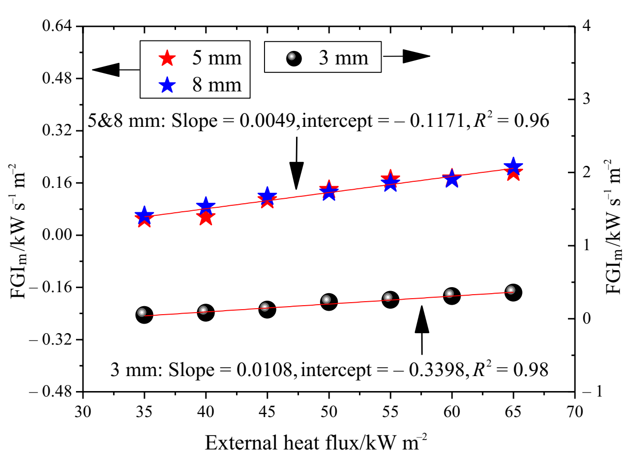

Fig. 9 FGI_m versus external heat flux under different thicknesses

where t_{pkHRR} denote the corresponding time when the peak HRR occurs (s).

Figure 9 shows the FGI for the maximum HRR FGI_m versus external heat flux under different thicknesses. More detailed information is presented in Table 6. As illustrated in Fig. 9 and Table 6, the FGI for the maximum HRR FGI_m increases with the external heat flux. Excellent linear relationship of FGI_m with the external heat flux is indicated. Furthermore, little differences occur between the values of FGI_m in the cases of 5 and 8 mm. Thus, the values of FGI_m in the cases of 5 and 8 mm may be correlated with the external heat flux together. It is similar to the case of the thermal thickness as illustrated in "Thermal thickness section". The large differences between the cases of 3 mm and 5, 8 mm are resulted by that the specimen with thickness of 3 mm is prone to be thermally thin material in which temperature distributes almost homogeneously when exposed to external heat [28]. However, the specimen with thickness of 5 and 8 mm may be considered as thermally thick material where heterogeneous temperature profile occurs when exposed to external heat [28]. The correlations for the thermally thick specimen (5 and 8 mm) and thermally thin specimen (3 mm) are expressed as Eqs. (19) and (20), respectively.

Table 6 FGI_m data under different thicknesses and external heat fluxes

External heat flux/ kW m^{-2}	FGI_m/kW s^{-1} m^{-2}		
	3 mm	5 mm	8 mm
35	0.0489	0.0493	0.0598
40	0.0809	0.0556	0.0878
45	0.1235	0.1079	0.1188
50	0.2262	0.1392	0.1314
55	0.2591	0.1714	0.1586
60	0.3084	0.1747	0.1714
65	0.3564	0.1922	0.2095

$$FGI_{mthick} = 0.0049\dot{q}''_e - 0.1171 \tag{19}$$

$$FGI_{mthin} = 0.0108\dot{q}''_e - 0.3398 \tag{20}$$

where FGI_{mthick} and FGI_{mthin} denote the FGI in the cases of thermally thick (5 and 8 mm) and thermally thin FRP (kW s^{-1} m^{-2}), respectively.

Conclusions

The present study investigates the ignition and combustion characteristics of phenolic fiber-reinforced plastic with different thicknesses using cone calorimeter under piloted ignition. Ignition time, thermal thickness, mass loss factor, MLR, HRR, THR, FPI and FGI are measured and analyzed. The major conclusions are summarized as follows:

1. The ignition time increases with the thickness and decreases with the external heat flux. Phenolic FRP with thickness of 3 mm may be considered as thermally

thin material, while phenolic FRP with thickness of 5 and 8 mm is prone to be thermally thick material. The critical heat flux, minimum heat flux and ignition temperature are deduced from the correlation of the ignition time with the external heat flux and validated.
2. The thermal thickness increases with the external heat flux. The value of the thermal thickness of phenolic FRP with thickness of 5 and 8 mm is almost the same under the identical external heat flux. Linear correlations of the thermal thickness with the ratio of the specimen density and the applied external heat flux under different thicknesses are demonstrated and presented.
3. Mass loss factor decreases with the thickness. There are three peak MLRs under low external heat fluxes, while there are merely two peak MLRs under high external heat fluxes. The average MLR increases with the external heat flux and the thickness. Linear correlations of the average MLR with the external heat flux under different thicknesses are demonstrated and presented.
4. The value of the average HRR of phenolic FRP with different thicknesses in the order of most to least is 8 mm > 3 mm > 5 mm. In addition, the average and maximum HRR increases with the external heat flux. Moreover, the maximum HRR increases with the thickness in the cases of external heat flux ≤ 45 kW m^{-2}. However, in the cases of external heat flux > 45 kW m^{-2}, the value of the maximum HRR of phenolic FRP with different thicknesses in the order of most to least is 8 mm > 3 mm > 5 mm. Linear correlations of the average and maximum HRR with the external heat flux under different thicknesses are demonstrated and presented.
5. The FPI for the maximum HRR increases with the external heat flux in the cases of 5 mm and 8 mm. However, little variations of the FPI for the maximum HRR with the external heat flux occur in the cases of 3 mm. The FGI for the maximum HRR increases with the external heat flux. The value of FGI for the maximum HRR of phenolic FRP with 5 and 8 mm is almost the same under the identical external heat flux. Linear correlations of FGI for the maximum HRR with the external heat flux under different thicknesses are demonstrated and presented.

Acknowledgements This work was sponsored by National Natural Science Foundation of China (No. 51806106) and Natural Science Foundation of Jiangsu Province, China (No: BK20170838).

References

1. An W, Jiang L, Sun J, Liew K. Correlation analysis of sample thickness, heat flux, and cone calorimetry test data of polystyrene foam. J Therm Anal Calorim. 2015;119(1):229–38.
2. Zhang B, Zhang J, Wang L, Xie H, Fan M. Investigation on effects of thickness on ignition characteristics and combustion process of the oil-impregnated transformer insulating paperboard. J Therm Anal Calorim. 2018;132(1):29–38.
3. Shi L, Chew MYL. Experimental study of woods under external heat flux by autoignition. J Therm Anal Calorim. 2013;111(2):1399–407.
4. Xu Q, Jin C, Jiang Y. Compare the flammability of two extruded polystyrene foams with micro-scale combustion calorimeter and cone calorimeter tests. J Therm Anal Calorim. 2017;127(3):2359–66.
5. Xu Q, Jin C, Griffin G, Jiang Y. Fire safety evaluation of expanded polystyrene foam by multi-scale methods. J Therm Anal Calorim. 2014;115(2):1651–60.
6. Xu Q, Jin C, Jiang Y. Analysis of the relationship between MCC and thermal analysis results in evaluating flammability of EPS foam. J Therm Anal Calorim. 2014;118(2):687–93.
7. Xu Q, Majlingova A, Zachar M, Jin C, Jiang Y. Correlation analysis of cone calorimetry test data assessment of the procedure with tests of different polymers. J Therm Anal Calorim. 2012;110(1):65–70.
8. Jiao C, Wang H, Chen X. Preparation of modified fly ash hollow glass microspheres using ionic liquids and its flame retardancy in thermoplastic polyurethane. J Therm Anal Calorim. 2018;10:1–10.
9. Shi L, Chew MYL. Fire behaviors of polymers under autoignition conditions in a cone calorimeter. Fire Saf J. 2013;61:243–53.
10. Li Z, Yuan T, Abu-Siada A, Masoum MAS, Li Z, Xu Y, et al. A new vibration testing platform for electronic current transformers. IEEE T Instrum Meas. 2019;68(3):704–12.
11. Li K, Pau DS, Wang J, Ji J. Modelling pyrolysis of charring materials: determining flame heat flux using bench-scale experiments of medium density fibreboard (MDF). Chem Eng Sci. 2015;123:39–48.
12. Mouritz A, Mathys Z. Post-fire mechanical properties of marine polymer composites. Compos Struct. 1999;47(1):643–53.
13. Mouritz A. Post-fire flexural properties of fibre-reinforced polyester, epoxy and phenolic composites. J Mater Sci. 2002;37(7):1377–86.
14. Avila MB. The effect of resin type and glass content on the fire engineering properties of typical FRP composites. Master thesis: University of California, Berkeley; 2007.
15. Hilal DemirbaŞ A. Yields and heating values of liquids and chars from spruce trunkbark pyrolysis. Energy Sources. 2005;27(14):1367–73.
16. Demirbas A. Determination of calorific values of bio-chars and pyro-oils from pyrolysis of beech trunkbarks. J Anal Appl Pyrolysis. 2004;72(2):215–9.
17. Ramsay G, Dowling V, McKechnie B, Leonard J. Methods for assessing the fire performance of phenolic resins and composites. Fire Saf Sci. 1995;2:355–66.
18. Duggan G. Usage of ISO 5660 data in UK railway standards and fire safety cases. In: A One-Day Conference on Fire Hazards, Testing, Materials and Products. Shrewsbury, UK: Rapra Technology Ltd.; 1997.
19. ISO-5660-1. Reaction-to-Fire Tests-Heat Release, Smoke Production and Mass Loss Rate-Part 1: Heat Release Rate (Cone Calorimeter Method). International Organization for Standardization Geneva, Switzerland; 2002.
20. ISO-17554. Reaction to Fire-Mass Loss Measurement. Geneva: International Organization for Standardization; 1998.
21. Quintiere J. A theoretical basis for flammability properties. Fire Mater. 2006;30(3):175–214.
22. Luche J, Rogaume T, Richard F, Guillaume E. Characterization of thermal properties and analysis of combustion behavior of PMMA in a cone calorimeter. Fire Saf J. 2011;46(7):451–61.

23. Luche J, Mathis E, Rogaume T, Richard F, Guillaume E. High-density polyethylene thermal degradation and gaseous compound evolution in a cone calorimeter. Fire Saf J. 2012;54:24–35.
24. Quang Dao D, Luche J, Richard F, Rogaume T, Bourhy-Weber C, Ruban S. Determination of characteristic parameters for the thermal decomposition of epoxy resin/carbon fibre composites in cone calorimeter. Int J Hydrog Energy. 2013;38(19):8167–78.
25. Babrauskas V. Ignition handbook: principles and applications to fire safety engineering, fire investigation, risk management and forensic science. 2nd ed. Issaquah: Fire Science; 2003.
26. Delichatsios MA. Piloted ignition times, critical heat fluxes and mass loss rates at reduced oxygen atmospheres. Fire Saf J. 2005;40(3):197–212.
27. Mikkola E, Wichman IS. On the thermal ignition of combustible materials. Fire Mater. 1989;14(3):87–96.
28. Mouritz AP, Gibson A. Fire properties of polymer composite materials. Dordrecht: Springer; 2007.
29. Chen R, Lu S, Li C, Li M, Lo S. Characterization of thermal decomposition behavior of commercial flame-retardant ethylene-propylene-diene monomer (EPDM) rubber. J Therm Anal Calorim. 2015;122:449–61.
30. Babrauskas V, Peacock RD. Heat release rate: the single most important variable in fire hazard. Fire Saf J. 1992;18(3):255–72.
31. Thornton W. The relation of oxygen to the heat of combustion of organic compounds. Lond Edinb Dublin Philos Mag J Sci. 1917;33(194):196–203.
32. Janssens M. Measuring rate of heat release by oxygen consumption. Fire Technol. 1991;27(3):234–49.